EXPERIMENTALLY DETERMINED METAL—OLIVINE ELEMENT PARTITIONING AND DIFFUSION IN OLIVINE WITH APPLICATIONS TO PALLASITES. Patrick H. Donohue[1]*, Eddy Hill[2], Gary R. Huss[1], and Michael J. Drake[2]; [1]Hawaii Institute of Geophysics and Planetology, University of Hawai'i at Mānoa, Honolulu, Hawaii 96822, USA; [2]Lunar and Planetary Laboratory, University of Arizona, Tucson, Arizona 85721, USA.

Introduction: Asteroids and planetesimals likely have core-mantle boundaries dominantly composed of high-Mg olivine and FeNi-metal [1,2]. Pallasite meteorites are thought to be disrupted remnants of these boundaries. This is supported by extremely slow cooling rates of ~1°C/Myr at low temperature, determined from diffusion profiles of taenite-kamacite contacts [3–5]. At higher temperatures (>800°C) where element diffusion in olivine occurs, minor element zonation (e.g., Ca, Cr, Co) suggests cooling rates four orders of magnitude faster at ~10,000°C/Myr [3,6–8]. This difference has long suggested a complex history for the formation of pallasites.

However, minor element diffusion in olivine is not well constrained for environmental conditions relevant to pallasites. For example, most previous experimental work determined metal-olivine partitioning or diffusion in silicate systems [9], for mono-element diffusion [10–12], or have to extrapolate to relevant temperature and oxygen fugacity (fO_2) [9,13,14]. Here, we determine metal—olivine element diffusion and partitioning behaviors of Fe, Ni, Co, Cr, and Mn at temperatures and oxygen fugacity conditions analogous to those during pallasite evolution. The new rates allow us to reconsider thermal evolution of pallasite meteorites.

Methods: Experimental work and preliminary analyses were conducted between 2005-2010 [15,16]. Briefly, experiments were conducted at 1 bar pressure, fO_2 of IW-1, and temperatures of 900 °C, 1300 °C, and 1550 °C for 354, 570, and 1532 hours, respectively. Synthetic olivine and metal compositional profiles were determined using electron microprobe analysis (EMPA) and secondary ion mass spectrometry (SIMS) analysis. Before each SIMS measurement, the spot was pre-sputtered for 2 to 5 minutes using a 15-25 µm raster and a 1 to 4 nA beam to eliminate surface contaminants. For measurements, the beam current was reduced to 0.25-0.5 nA (5-10 µm spot diameter) and the raster reduced to ~5 µm. Typical measurement spots were 7-10 µm in diameter.

For EBSD measurements, five to ten point analyses were conducted on each FeNiCo sample to ensure single crystals were analyzed. The SEM was operated at low vacuum (11 Pa) with 20 kV accelerating voltage, 5 nA beam current and 70° tilted stage. EBSD methods are described in detail in [17].

Results: The use of pure forsterite as starting material meant that all elements of interest diffused into the olivine from the metal, yielding positive diffusion profiles. Dissolution of olivine was not significant, but Mg-wüstite precipitated on several crystal margins.

Diffusion rates. Metal acts as a concentration buffer, thus the system can be treated as one-dimensional diffusion in a semi-infinite medium. When diffusion rate D ($cm^2\ s^{-1}$) is independent of concentration, Fick's Law can be solved by implementing the error function (*erf*):

$$\mathrm{erf}^{-1}(C - C_0)/(C_i - C_0) = x / \sqrt{(4D^*t)}; \quad (1)$$

where C is the concentration (ppm) at distance x (cm) from the interface, C_0 is the farfield composition in olivine, C_i is the interface concentration, and time t is the experimental duration (seconds). A non-linear least-squares solution was used to solve for C_i and D simultaneously (Fig. 1). Our new Fe, Ni, Co, and Mn diffusion rates are similar to one another, suggesting similar diffusion behavior in the metal-olivine system. Chromium is the only outlier, exhibiting a shallower slope in Fig 1. Although we did not find a statistically significant difference between the diffusion rates determined for the a, b, and c axes, there was an indication the diffusion rates may be faster along the c axis (as reported by [18,19]).

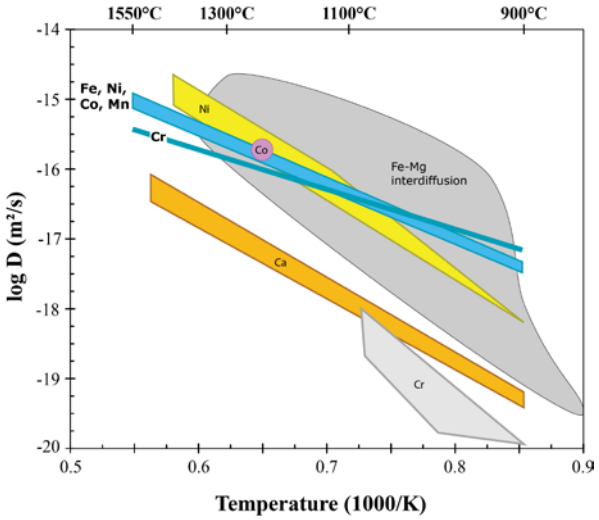

Fig. 1: Arrhenius diagram and fields of determined diffusion parameters from our olivine experiments (bold labels, blue lines) at IW-1, compared to literature ranges [18,19].

Partition coefficients. Partition coefficients ($K_M^{met/ol}$) were calculated as the ratio of normalized cations of *M* (mol. %) in metal to *M* in olivine at the interface (C_i) (Table 1). The increase from Fe < Co < Ni at high temperatures is consistent with previous findings [8].

Table 1. Partition coefficients ($K_M^{met/ol}$) and 2σ uncert.

Temp.	**900°C**	**1300°C**	**1550°C**
K_{Cr}	0.04 ± 0.01	0.09 ± 0.01	0.17 ± 0.02
K_{Mn}	0.0041 ± 0.0004	0.0069 ± 0.0005	0.009 ± 0.001
K_{Fe}	54 ± 3	47 ± 1	32.0 ± 0.4
K_{Co}	506 ± 56	443 ± 77	288 ± 7
K_{Ni}	386 ± 22	1960 ± 386	2472 ± 184

Discussion: Pallasite olivines often exhibit distinct zonation profiles for minor elements. From core to rim, some elements decrease significantly (e.g., Ca, Cr, and Ni) or show small decreases (e.g., Fe) [6,8]. In contrast, the profile for Mn is relatively flat, and may actually increase at the very margins of some olivines [2,8]. These differences are typically assumed to be diffusion-driven, where diffusion rates for Fe and Mn are faster than, for example, Cr and Ni. However, we found diffusion rates were similar for the transition metals Fe, Ni, Co, and Mn over a range of temperatures. Thus, we suggest pallasite zonation profiles are controlled by changing boundary conditions. The most likely scenario involves progressive re-equilibration of olivine with minor phases or metal affected by crystallization of new phases. Indeed, metal compositions in equilibrium with olivine rims (c.f, [6]), calculated using the new K_M values, are consistent with approaches to equilibrium at ≥1300°C. The ubiquity of chromite suggests a sink for Cr during re-equilibration, whereas Mn has no such minor phase to act as a sink. Indeed, late stage increase in Mn activity is recorded in high-Mn phosphoran olivine rims on some pallasite olivines [2,20]. This may be tied to isolated melt packets with higher Si activity and correspondingly higher P and Mn activity, tied with higher fO_2 [2,19] to drive these changes.

Pallasites likely formed and cooled below ~600°C within ~10 Myr of the solar system [2], and thermal metamorphism has not subsequently altered the rocks. The extent of zonation would be controlled by the time spent above the closure temperature of diffusion. Using Dodson's formulation for closure temperature [21], we calculated olivine would close to diffusion after cooling below ~700°C (similar to refs. [2,5]). Using Ni and Cr zonation profiles for several pallasite olivines in Albin and Eagle Station [6], we used the new diffusion rates and *Equation 1* to determine the time required for the profiles to form. At low-temperatures, where diffusion is slowest but still active (~700°C), we calculate timescales of ~0.02 Myr. The required time would be even less at higher temperatures where diffusion is faster. This suggests that zonation is formed over a short timescale relative to the overall cooling of pallasites. As early-formed solar system objects, pallasites may hold records of short-lived radionuclides (e.g., ^{53}Mn). The ^{53}Mn-^{53}Cr system can be useful in dating objects formed during the first ~20 Myr of solar system history. Our results suggest the cores of large pallasite olivines may retain an early solar system signature.

Conclusions: Metal—olivine element partitioning and diffusion behaviors were determined at low fO_2 and for a range of subsolidus temperatures analogous to pallasite olivine thermal history. Pallasite olivine cores reflect initial high-temperature equilibration, whereas rim zonation is the result of partial re-equilibration during changing boundary conditions (e.g., metal composition). However, diffusion rates suggest this re-equilibration occurred over short timescales relative to overall pallasite cooling, likely tied to faster initial cooling rates.

Acknowledgments: This work was supported by the NASA Cosmochemistry program (NNX08-AG58G and NNX14-AI19G to G.R.H.; NNX07-A152G to M.J.D.).

References: [1] Mason B. H. (1962) *Meteorites*. [2] Boesenberg J. S. et al. (2012) *GCA*, 89, 134–158. [3] Buseck P. R. and Goldstein J. I. (1969) *GSA Bull.*, 80, 2141–2158. [4] Short J. M. and Goldstein J. I. (1967) *Science*, 156, 59–61. [5] Wasson J. T. and Choi B.-G. (2003) *GCA*, 67, 3079–3096. [6] Hsu W. (2003) *MaPS*, 38, 1217–1241. [7] Tomiyama T. and Huss G. R. (2006) *LPSC*, XXXVII, #2132. [8] Miyamoto M. (1997) *JGRP*, 102, 21613–21618. [9] Ehlers K. et al. (1992) *GCA*, 56, 3733–3743. [10] Cherniak D. J. and Van Orman J. A. (2014) *GCA*, 129, 1–12. [11] Cherniak D. J. and Liang Y. (2014) *GCA*, 147, 43–57. [12] Coogan L. A. et al. (2005) *GCA*, 69, 3683–3694. [13] Bédard J. H. (2005) *Lithos*, 83, 394–419. [14] Cottrell E. et al. (2009) *EPSL*, 281, 275–287. [15] Hill E. et al. (2010) *LPSC*, 41, #1911. [16] Hill E. et al. (2008) *LPSC*, 39, #1415. [17] Brugger C. R. and Hammer J. E. (2015) *Am. Mineral.*, 100, 385–395. [18] Brady J. B. and Cherniak D. J. (2010) *RiMG*, 72, 899–920. [19] Zhukova I. et al. (2014) *CMP*, 168, 1–15. [20] McKibbin S. J. et al. (2013) *GCA*, 119, 1–17. [21] Dodson M. H. (1973) *CMP*, 40, 259–274.